Abdominal Radiology (2019) 44:1470–1480
https://doi.org/10.1007/s00261-018-1848-x

KIDNEYS, URETERS, BLADDER, RETROPERITONEUM

Juxtatumoral perinephric fat analysis in clear cell renal cell carcinoma

Tania S. Gill[1] · Bino A. Varghese[1] · Darryl H. Hwang[1] · Steven Y. Cen[1] · Manju Aron[2] · Monish Aron[3] · Vinay A. Duddalwar[1]

Published online: 30 November 2018

Abstract

Purpose The purpose of the study was to evaluate the feasibility of using contrast-enhanced computed tomography (CECT)-based texture analysis (CTTA) metrics to differentiate between juxtatumoral perinephric fat (JPF) surrounding low-grade (ISUP 1–2) versus high-grade (ISUP 3–4) clear cell renal cell carcinoma (ccRCC).

Methods In this IRB-approved study, we retrospectively queried the surgical database between June 2009 and April 2016 and identified 83 patients with pathologically confirmed ccRCC (low grade: $n = 54$, mean age = 61.5 years, 18F/35M; high grade $n = 30$, mean age = 61.7 years, 8F/22M) who also had pre-operative multiphase CT acquisitions. CT images were transferred to a 3D workstation, and nephrographic phase JPF regions were manually segmented. Using an in-house developed Matlab program, a CTTA panel comprising of texture metrics extracted using six different methods, histogram, 2D- and 3D-Gray-level co-occurrence matrix (GLCM) and Gray-level difference matrix (GLDM), and 2D-Fast Fourier Transform (FFT) analyses, was applied to the segmented images to assess JPF textural heterogeneity in low- versus high-grade ccRCC. Univariate analysis and receiver-operator characteristics (ROC) analysis were used to assess interclass differences in texture metrics and their prediction accuracy, respectively.

Results All methods except GLCM consistently revealed increased heterogeneity in the JPF surrounding high- versus low-grade ccRCC. FFT showed increased complexity index ($p < 0.01$). Histogram analysis showed increased kurtosis and positive skewness in ($p < 0.03$), and GLDM analysis showed decreased measure of correlation coefficient (MCC) ($p < 0.04$). Several of the GLCM metrics showed statistically significant ($p < 0.04$) textural differences between the two groups, but with no consistent trend. ROC analysis showed that MCC in GLCM analysis had an area under the curve of 0.75.

Conclusions Our study suggests that CTTA of ccRCC shows statistically significant textural differences in JPF surrounding high- versus low-grade ccRCC.

Keywords Perinephric fat · CcRCC · Texture · Radiomics · Renal mass · Tumor grade

Introduction

Approximately 65,340 new cases of kidney cancer will occur in 2018 [1]. Renal cell carcinoma (RCC) and its subtypes (most commonly clear cell, papillary, chromophobe) will make up 90% of these cases. Compared to other subtypes, clear cell renal cell carcinoma (ccRCC) is the most common, but also has the worse prognosis [2]. Inherent genetic differences contribute to disparate phenotypes amongst, and even within, tumor subtypes [3]. Different phenotypes can, on occasion, be seen on gross pathology; to wit, ccRCC is commonly a solid, encapsulated mass with necrotic and hemorrhagic changes,

✉ Vinay A. Duddalwar
vinay.duddalwar@med.usc.edu

[1] Keck School of Medicine, University of Southern California, Radiology, Los Angeles, CA 90033, USA

[2] Norris Comprehensive Cancer Center, Keck School of Medicine, University of Southern California, Pathology, Los Angeles, CA, USA

[3] Keck School of Medicine, USC Institute of Urology, University of Southern California, Los Angeles, CA, USA

whereas papillary tumors are not uncommonly mixed cystic and solid [4].

Just as renal tumor cells undergo pathologic changes, we hypothesized that the juxtatumoral perinephric fat (JPF) adjacent to a malignant tumor may develop responsive changes due to its proximity. Evidence of cancer characteristics being reflected in adjacent, histologically normal tissue has been noted in other cancers, such as breast [5, 6]. We explored whether imaging characteristics of the JPF next to the renal mass can contribute towards the radiologic diagnosis of the underlying renal malignancy.

To date, we were unable to find any publications assessing textural characteristics of JPF in patients with RCC. While some studies have evaluated JPF as an indicator of operative complexity during PN, none have explored whether JPF can itself serve as a quantitative metric to aid in radiologic evaluation of RCC [7–9]. To address this question, we evaluated pre-operative multiphase CT scans of patients with pathologically confirmed ccRCC, focusing on the JPF. Specifically, we evaluated the feasibility of using contrast-enhanced computed tomography (CECT)-based texture analysis (CTTA) metrics to differentiate between juxtatumoral perinephric fat (JPF) surrounding low-grade (ISUP 1–2) versus high-grade (ISUP 3–4) ccRCC.

Subjects/patients and methods

Patient selection

After institutional review board (IRB) approval and informed consent, a total of 83 patients were retrospectively identified from our prospectively maintained surgical database who had undergone pre-operative multiphase CECT imaging of the abdomen followed by radical (n = 15) or partial (n = 68) nephrectomy surgery from June 2009 to April 2016 for pathologically confirmed ccRCC. Pathologic evaluation was performed by specialized genitourinary pathologists, and histologic grade was defined according to the International Society of Urological Pathology (ISUP). Inclusion criteria comprised patients with pathologically confirmed ccRCC, and renal mass CECT study performed at the University of Southern California (USC). Exclusion criteria comprised benign lesions, non-clear cell RCC and non-availability of pre-op CECT. For patients with bilateral (n = 2) or multiple renal tumors (n = 6), we selected only the tumor with the largest diameter for inclusion.

Image acquisition

All CT (Brilliance 64, Philips Healthcare, CT) scans were obtained during patient breath-holding with the following parameters: 120 kVp, variable tube current, slice thickness of 0.5 mm with reconstruction interval of 2 mm Approximately 100–150 mL of non-ionic water soluble intravenous iodinated contrast (Isovue 350, Bracco Imaging) dosed to weight was administered with a power injector at a rate of 4–5 mL/s. 4 phase were obtained: Pre-contrast (0 s), corticomedullary (25 s), nephrographic (90 s), and excretory (5 min) phases.

CT analysis

Multiphase CT images were transferred to a three-dimensional workstation (Synapse 3D; Fujifilm Medical Systems, Stamford, CT). JPF surrounding the renal tumor was segmented by the same reader in Synapse 3D as regions of interest (ROIs) using a tumor ROI dilation and subtraction method (Fig. 1). First we dilated out 5 pixels on average from tumor, to encompass the JPF (Fig. 1a). Then we made an additional image dilated out 1 pixel from the tumor, in order to remove the tumor from the ROI (Fig. 1b). Subtraction of these two images yielded an ROI encompassing mainly the JPF (Fig. 1c). Extraneous components (non-perinephric fat voxels: renal parenchyma, bowel, liver, vasculature, lymph nodes, adjacent visceral and muscular tissue) were manually deleted so that our ROI would contain only the JPF (Fig. 1d). Segmentation was performed on the nephrographic phase. Manual segmentation of the perinephric fat was performed on all images where the tumor was seen.

Multi-phase CT volumes were co-registered to the nephrographic phase using the Statistical Parametric Mapping software package. Custom MATLAB (Mathworks, Natick, MA) code was used to extract voxel data corresponding to the ROI. 2D CTTA analysis was conducted on the JPF area extracted from the orientations that provided the largest tumor diameter in each phase in the axial, coronal or sagittal dimension. 3D CTTA analysis was conducted on the whole JPF volume.

Radiomics analysis

From the co-registered CECT scans, we applied a panel of tissue characterization algorithms (radiomics panel) to extract texture-based imaging metrics. Specifically, 6 different types of texture extraction techniques were used on each CECT phase of each tumor image with 29 different texture metrics assessing the inherent JPF heterogeneity. The techniques are well described in literature [10]; here, we provide a summary (Table 1). *Histogram analysis (1st order statistics)* The mean and median absolute enhancement and histogram distribution parameters skewness, kurtosis, standard deviation, and interquartile range were computed for JPF surrounding each lesion on all phases.

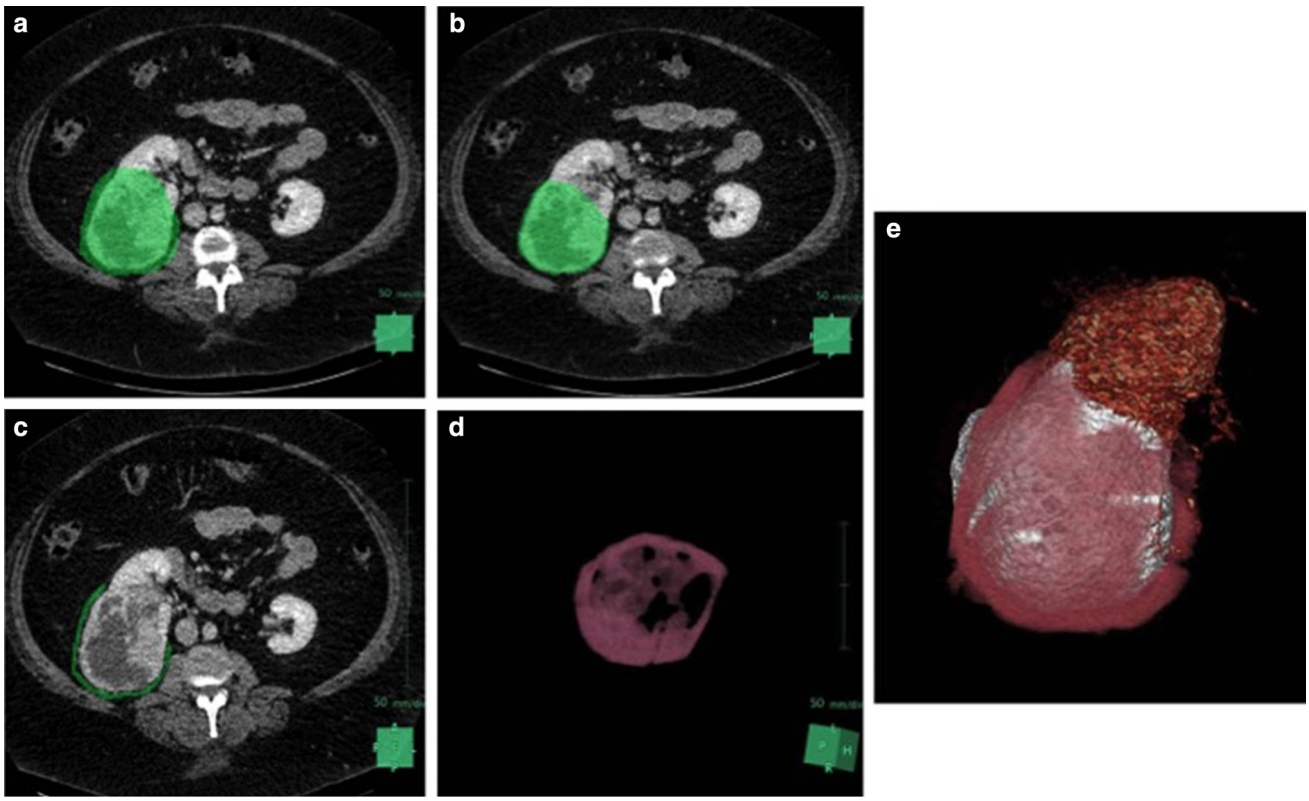

Fig. 1 Nephrographic phase CECT image of right-sided grade 2 ccRCC lesion illustrating ROI acquisition. **a** The green mask was dilated out 5 pixels to encompass surrounding JPF. **b** On another copy of the image, the green mask was dilated out 1 pixel to encompass the tumor. **c** Subtraction of image (**b**) from (**a**) yielded ROI with JPF. **d** Di-COM image of ROI after manual removal of non-perinephric fat voxels. **e** 3D rendered image illustrating our JPF ROI (pink) surrounding the renal tumor (white)

Table 1 Radiomics analysis parameters

Histogram analysis	GLCM/GLDM	Spectral analysis
Kurtosis	Angular second moment	Entropy of FFT mag
Mean	Contrast	Entropy of FFT phase
Quartile range	Correlation	Complexity index
Standard deviation	Dissimilarity	
Skewness	Entropy	
Median	Homogeneity	
	Inverse difference moment mean	
	Information measures of correlation 1 and 2 mean	
	Measure of correlation coefficient	
	Square root of variance	
	Standard deviation	
	Uniformity	
	Variance	
	Difference average and entropy	
	Sum of average, entropy, and variance	
	Mean	

Texture metrics (second to higher order statistics) We performed 2D- and 3D- Gray-level co-occurrence method (GLCM) and Gray-level difference method (GLDM) and 2D Fourier transform analysis. Haralick texture metrics such as angular second moment, contrast, correlation, dissimilarity, entropy, homogeneity, inverse difference moment, information measures of correlation q and 2 means, measure of correlation coefficient, square root of variance, standard deviation, uniformity, variance, difference average and entropy, sum of average, entropy and variance and mean were calculated from all GLCM and GLDM maps. From the Fourier transform (Fast-Fourier transform-based, FFT) analysis, metrics such as complexity index (sum of all tumor frequency magnitude), entropy of FFT magnitude and phase were extracted from the JPF surrounding each lesion on all phases [10].

Statistical analysis

We analyzed the data in two separate categories: JPF surrounding low-grade (ISUP grade 1–2) and JPF surrounding high-grade (ISUP grade 3–4) in all phases. Independent *t* test or Wilcoxon rank sum test depending on data normality were used as exploratory univariate analysis to compare parameters between the two categories. ROC curve analysis was used to assess prediction accuracy when distinguishing the JPF surrounding low-grade versus high-grade ccRCC. p values < 0.05 were viewed as statistically significant.

Table 2 Tumor characteristics

	Low-grade (1–2)	High-grade (3–4)
Tumor size		
Mean ± SD	3.40 ± 1.80	4.33 ± 2.24
Median (IQR)	3.15 (2.4–4.1)	3.6 (2.8–4.9)
Exophytic/endophytic		
≥ 50% Exophytic	26 (48%)	10 (35%)
< 50% Exophytic	23 (43%)	16 (55%)
Entirely endophytic	5 (9%)	3 (10%)
Path stage[a]		
pT1a	33 (61%)	16 (57%)
pT1b	7 (13%)	4 (14%)
pT2a	2 (4%)	0
pT3a	12 (22%)	7 (25%)
pT3b	0	1 (4%)

[a]For 1 high-grade lesion, the path stage was not recorded

Results

Patient and tumor characteristics

Between June 2009 and April 2016, 83 patients (57 male, 26 female) with pathologically confirmed ccRCC tumors who had pre-operative multiphase phase CT images were included in our study. There were 42 left-sided lesions and 41 right-sided lesions. ISUP grades were grouped as follows: low-grade (1–2; $n = 53$) and high-grade (3–4; $n = 30$). Tumor characteristics are detailed in Table 2.

Characteristics of the JPF surrounding ccRCC

We assessed JPF characteristics using Fourier, GLCM, GLDM, and Histogram analysis variables; for clarity purposes, we only reported those variables that were statistically significant.

In the Fourier analysis (Table 3), the FFT-based metric: complexity index, in all planes (axial, sagittal, coronal) was statistically significant ($p < 0.01$). The mean sum frequency was less in all planes for JPF surrounding low-grade as compared to high-grade (axial, 457E6 vs 496E6, $p < 0.01$; sagittal, 437E6 vs 48E7, $p < 0.01$; coronal, 407E6 vs 437E6, $p < 0.01$) ccRCC. Axial and sagittal complexity index were the most normally distributed variables (Fig. 2).

In the GLCM analysis (Table 4), JPF-based texture metrics in the nephrographic phase that were statistically significant ($p < 0.05$) did not show consistent heterogeneous trends in regard to both groups. In the sagittal plane, JPF surrounding low-grade ccRCC had on an average lower values when compared to JPF surrounding high-grade ccRCC for texture metrics: measure of correlation coefficient (0.64 vs 0.71, $p = 0.012$), uniformity (0.1 vs 0.11, $p = 0.027$), homogeneity (0.28 vs 0.31, $p = 0.015$), and difference of average (− 6.57 vs − 5.05, $p = 0.016$). In contrast, JPF surrounding low-grade ccRCC had higher mean values when compared to JPF surrounding high-grade ccRCC for texture metrics: contrast (17.14 vs 13.12, $p = 0.016$), dissimilarity (3.17 vs 2.77, $p = 0.018$), and difference of entropy (2.14 vs 2.05, $p = 0.028$). Between both groups, angular second moment was comparable (0.01 vs 0.01, $p = 0.027$). In the coronal plane (Table 4), JPF surrounding low-grade ccRCC had higher mean values when compared to JPF surrounding high-grade ccRCC for texture metrics: square of variance (65.18 vs 54.75, $p = 0.032$), standard deviation (7.92 vs 7.28, $p = 0.032$), mean (8.15 vs 7.48, $p = 0.037$), and sum of average (16.30 vs 14.96, $p = 0.037$). Between both groups, inverse difference moment (0.01 vs 0.01, $p = 0.021$) was comparable.

Table 3 Fourier analysis parameters of JPF

Complexity index	Grade 1–2 (n = 54)	Grade 3–4 (n = 30)	p value
Axial			<0.01
Mean ± SD	457E6 ± 148E6	496E6 ± 165E6	
Median (IQR)	46E7 (348E6; 545E6)	512E6 (357E6; 614E6)	
Sagittal			<0.01
Mean ± SD	437E6 ± 135E6	48E7 ± 143E6	
Median (IQR)	424E6 (362E6; 513E6)	458E6 (371E6; 575E6)	
Coronal			<0.01
Mean ± SD	407E6 ± 4E7	437E6 ± 147E6	
Median (IQR)	401E6 (35E7; 478E6)	39E7 (338E6; 536E6)	

Complexity Index refers to sum of all tumor frequency magnitude

SD standard deviation, *IQR* interquartile range, *E* exponent

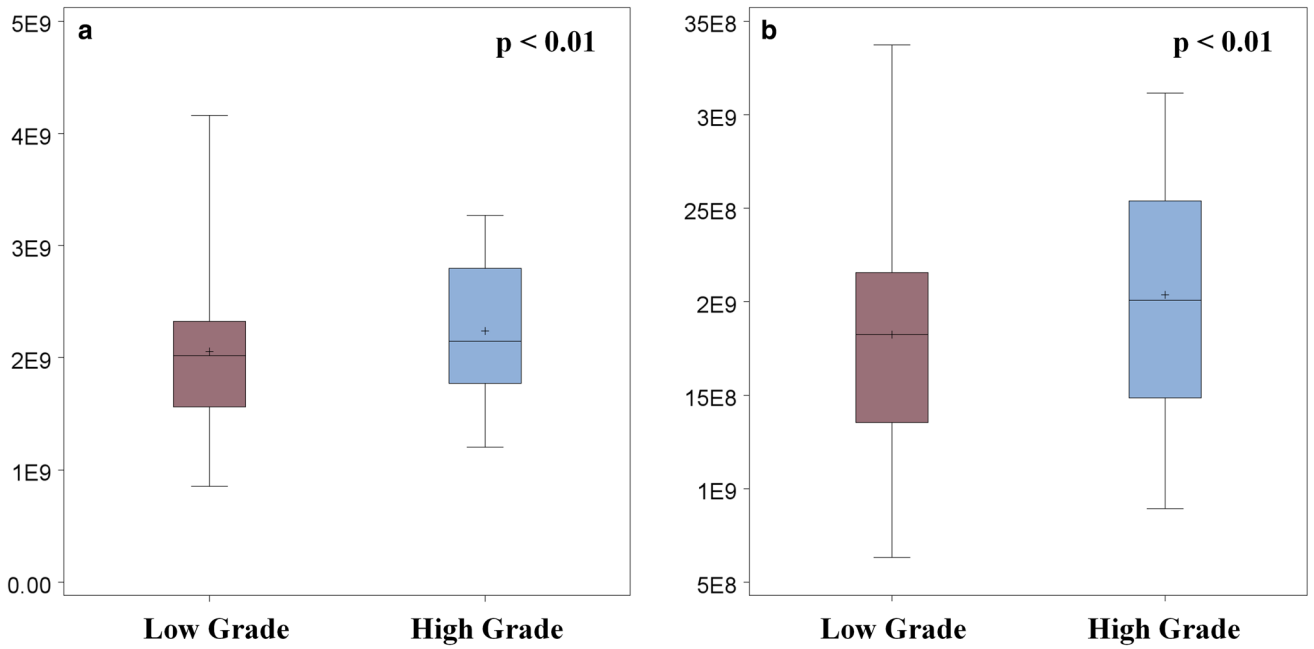

Fig. 2 Fourier analysis boxplots of JPF. Low grade: ISUP Grade 1 and 2; high grade: ISUP Grade 3 and 4. **a** Axial complexity index, $p < 0.01$. **b** Sagittal complexity index, $p < 0.01$

While GLCM metrics were significantly different, there was no trend in our results.

In the GLDM analysis (Fig. 3), the only parameter that was statistically significant was the texture metric: measure of correlation coefficient in the coronal plane. The mean measure of correlation coefficient was higher in JPF surrounding low-grade lesions compared to high-grade lesions (0.89 vs 0.76, $p = 0.038$).

Histogram-analysis based variables (Table 5) that were found to be significant were skewness and mean. For skewness, we found higher mean values in the JPF surrounding high-grade group compared to the low-grade group (0.65 vs 0.40, $p = 0.015$). For mean, we found lower mean values in the JPF surrounding high-grade group compared to low-grade group (7.02 vs 7.72, $p = 0.028$). Box plots for these two variables are shown in Fig. 4.

We conducted ROC analysis for all radiomic metrics showing statistically significant ($p < 0.05$) difference between high- and low-grade tumors based on the univariate analysis. Of these, the best supportive ROC analysis reported an area under the under the curve (AUC) of 0.75 with a 95% confidence interval (0.63–0.86) showing discrimination of JPF surrounding low-grade versus high-grade ccRCC using the GLCM-based texture metric: correlation coefficient assessed in the sagittal orientation (Fig. 5).

Table 4 GLCM parameters of JPF

	Grade 1–2 (n = 54)	Grade 3–4 (n = 30)	p value
Sagittal			
MCC			
Mean ± SD	0.64 ± 0.13	0.71 ± 0.12	< 0.02
Median (IQR)	0.69 (0.52–0.97)	0.66 (0.52–1.01)	
Uniformity			
Mean ± SD	0.1 ± 0.02	0.11 ± 0.2	< 0.03
Median (IQR)	0.11 (009–0.12)	0.10 (0.09–0.12)	
HOM			
Mean ± SD	0.28 ± 0.05	0.31 ± 0.05	< 0.02
Median (IQR)	0.25 (0.21–0.27)	0.23 (0.19–0.28)	
difAVE			
Mean ± SD	− 6.57 ± 3.36	− 5.05 ± 1.97	< 0.02
Median (IQR)	− 25.3 (− 65.1 to − 9.55)	− 39 (− 118 to − 11.5)	
CON			
Mean ± SD	17.14 ± 8.36	13.12 ± 5.64	< 0.02
Median (IQR)	52.81 (21.64–113.6)	75.45 (24.16–192)	
DIS			
Mean ± SD	3.17 ± 0.75	2.77 ± 0.62	< 0.02
Median (IQR)	3.07 (2.64–3.67)	2.72 (2.36–3.17)	
difENT			
Mean ± SD	2.14 ± 0.19	2.05 ± 0.19	< 0.03
Median (IQR)	2.61 (2.33–2.90)	2.84 (2.35–3.15)	
ASM			
Mean ± SD	0.01 ± 0.01	0.01 ± 0.01	< 0.03
Median (IQR)	0.01 (0.01–0.02)	0.01 (0.01–0.02)	
Coronal			
SQV			< 0.04
Mean ± SD	65.18 ± 26.61	54.75 ± 22.64	
Median (IQR)	59.16 (49.50–78.33)	51.01 (41.32–61.63)	
StdDev			
Mean ± SD	7.92 ± 1.56	7.28 ± 1.37	< 0.04
Median (IQR)	7.69 (7.04–8.85)	7.14 (6.43–7.85)	
Mean			
Mean ± SD	8.15 ± 1.62	7.48 ± 1.38	< 0.04
Median (IQR)	8.05 (7.25–8.95)	7.36 (6.52–8.21)	
sumAve			
Mean ± SD	16.30 ± 3.23	14.96 ± 2.77	< 0.04
Median (IQR)	16.09 (14.5–17.91)	14.72 (13.03–16.42)	
IDM			
Mean ± SD	0.01 ± 0.01	0.01 ± 0.01	< 0.03
Median (IQR)	0.01 (0.01–0.01)	0.01 (0.01–0.02)	

Data reported as mean ± standard deviation, median (IQ)

MCC measure of correlation coefficient, *HOM homogeneity*, *difAve* difference of average, *CON* contrast, *DIS* dissimilarity, *difENT* difference of entropy, *ASM* angular second moment, *SQV* sum of squares variance, *StdDev* standard deviation, *sumAve* summary of average, *IDM* inverse difference moment

Discussion

In this paper, we present results showing that radiomic analysis of JPF adjacent to cRCC tumors can be used to differentiate high-grade from low-grade tumors. We identified key quantitative imaging-metrics from routine clinical-data that were significantly different between JPF surrounding high- versus low-grade ccRCC. Receiver operator characteristics analysis revealed an area under the curve (AUC) of 0.75 with a 95% confidence interval (0.63–0.86), demonstrating the possibility that an underlying renal malignancy may elicit radiologically identifiable changes in the JPF. To our knowledge, our study is the first to explore this concept.

Current clinical imaging is geared primarily towards identifying anatomical information. There is recognition that radiomic analysis can add quantitative discrimination which helps in characterizing lesions further in terms of histologic grades and types. Particularly, texture analysis has been identified as a novel and promising tool to assist in differentiating various renal tumors [11]. Textural characteristics of RCC subtypes have been shown to correlate with their oncologic potential [3].

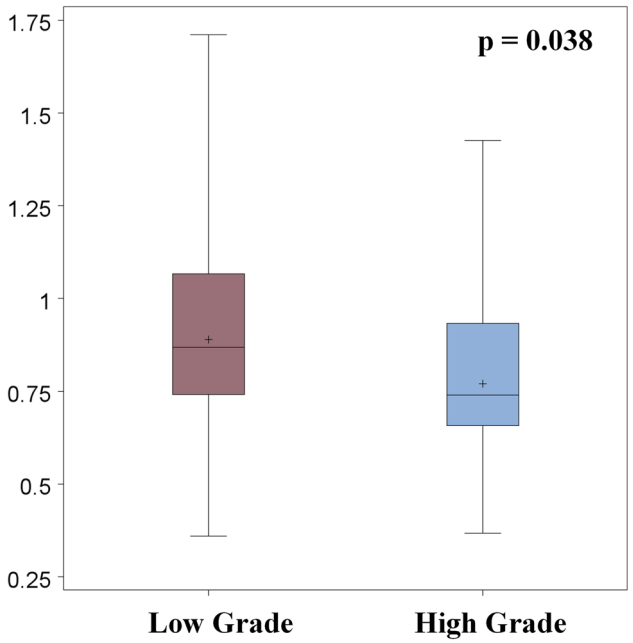

Fig. 3 GLDM measure of correlation coefficient of JPF. Low grade: ISUP Grade 1 and 2; high grade: ISUP Grade 3 and 4

While characterizing RCC lesions by evaluating the JPF, we observe that the most statistically significant ($p < 0.05$) metrics that show differences between the JPF adjacent to low-grade and high-grade lesions are Fourier analysis, GLDM and Histogram analysis. In general, previous investigators have reported kurtosis (or the magnitude of histogram of gray-levels) and skewness (skewness of the histogram of image gray-levels) features as quantitative metrics of tumor heterogeneity. Higher kurtosis and positive value of skewness have been associated with treatment failure, while lower values indicate a response to treatment [12]. In our study, high skewness (higher heterogeneity) was observed in the JPF surrounding high-grade tumors, which is concordant with previous studies [13].

The GLDM describes pair-wise arrangement of pixels with the set absolute difference in gray-level, in a given direction and distance, and used to highlight local heterogeneity information. Of the various GLDM metrics, measure of correlation coefficient (MCC) showed statistically significant difference between the JPF surrounding low- versus high-grade ccRCC. The MCC of JPF surrounding the high-grade tumor was significantly lower than the MCC of the JPF surrounding the low-grade tumor ($p = 0.038$). This indicates that the JPF surrounding high-grade ccRCC is more spatially heterogeneous (less correlated to each other) than the JPF surrounding low-grade ccRCC, which is in accordance with literature and corroborate the results we obtained using the histogram analysis metrics [10, 14].

Fast Fourier analysis of the JPF surrounding the ccRCC showed significant difference in heterogeneity of the frequencies making up the JPF ROIs, captured by the complexity index measure (sum of the spatial frequencies making up the JPF ROIs). The complexity index of the JPF surrounding the high-grade ccRCC was significantly ($p < 0.01$) higher than the JPF surrounding the low-grade ccRCC. This is in accordance with observation of higher complexity index of high-grade ccRCC compared to low-

Table 5 Histogram analysis parameters (skewness, mean) of JPF

	Grade 1–2 ($n = 54$)	Grade 3–4 ($n = 30$)	p value
Skewness			< 0.02
Mean ± SD	0.40 ± 0.61	0.65 ± 0.34	
Median (IQR)	0.41 (0.18–0.68)	0.60 (0.42–0.83)	
Mean			< 0.03
Mean ± SD	7.72 ± 1.66	7.04 ± 1.48	
Median (IQR)	7.42 (6.82–8.36)	6.82 (6.21–7.79)	

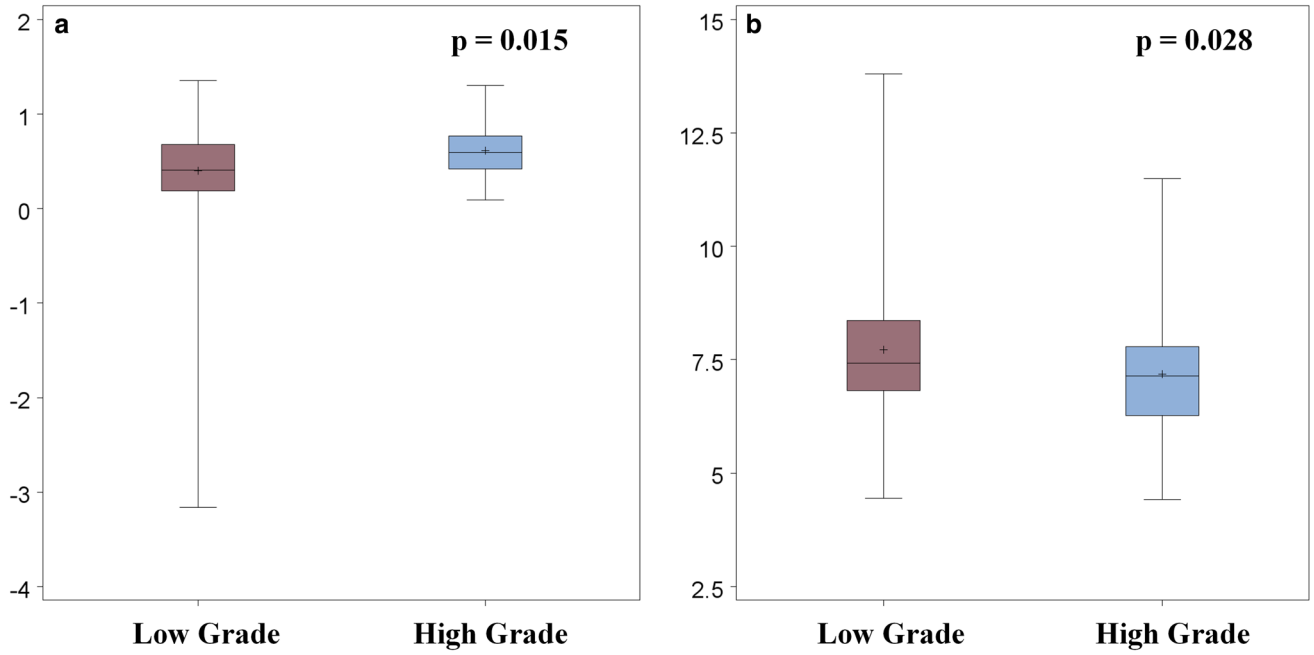

Fig. 4 Histogram analysis boxplots of JPF. Low grade: ISUP Grade 1 and 2; high grade: ISUP Grade 3 and 4. **a** Skewness, $p = 0.015$. **b** Mean, $p = 0.028$

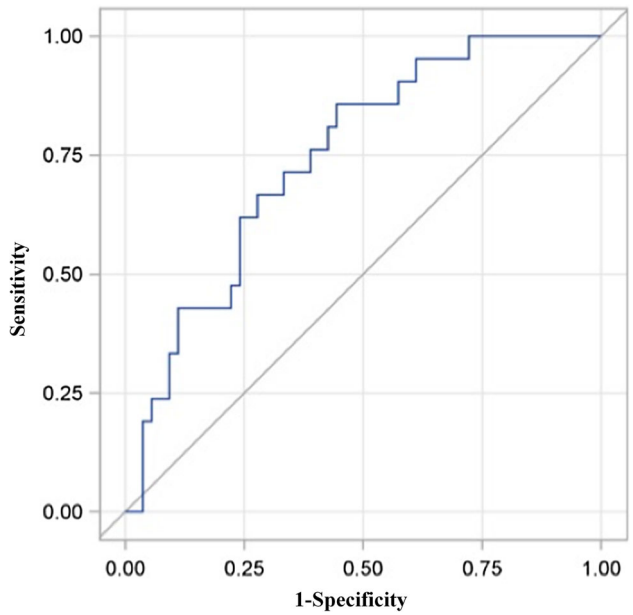

Fig. 5 ROC curve based on GLCM measure of correlation coefficient on sagittal plane. Area under the curve (AUC) = 0.7460 with 95% CI 0.63–0.86

grade ccRCC tumors [10] and corroborates the results we obtained using the histogram analysis metrics.

GLCM describes pair-wise arrangement of pixels with the same gray-level, in a given direction and distance, and is used to highlight local heterogeneity information. In our analysis, GLCM metrics showing textural heterogeneity, such as angular second moment, contrast, dissimilarity, inverse difference moment mean, measure of correlation coefficient, square root of variance, standard deviation, variance, difference average and entropy, sum of average and mean, have lower values for JPF surrounding high-grade compared to low-grade tumors. In addition, metrics measuring tumor homogeneity, such as homogeneity and uniformity, show higher values for JPF surrounding high-grade tumor compared to low-grade tumor. The underlying reasoning behind this contradictory observation needs to be further evaluated. A plausible reason may be the non-optimized number of gray-levels chosen to represent the image, which are typically chosen based on a co-optimization of relevance and accuracy of the texture metric.

Across all the texture methods we evaluated, results from Histogram analysis, Fourier analysis, and GLDM based texture analysis are concordant with recent studies by Scheida et al., showing increased textural heterogeneity among high-grade compared to low-grade chRCC tumors [15]. In addition, prior studies by Lopez et al. exploring the cellular make-up of ccRCC report higher intratumoral heterogeneity in high grade and stage ccRCC [16]. In our study, the increased heterogeneity of the JPF adjacent to high-grade ccRCC as quantified by the CTTA panel may be attributed to increased neoangiogenesis and/or necrosis of the JPF surrounding high-grade ccRCC compared to low-grade ccRCC [3]. Another possibility is the attraction or aggregation of inflammatory cells in the peritumoral tissues as a response to the neoplasm [17]. Additionally, increased density in the peritumoral tissue may also reflect

increased collateral supply from the perirenal and capsular vessels [3].

While metrics such as adhesive perirenal fat (APF) and the Mayo adhesive probability (MAP) score have analyzed perinephric fat as a measure for assessing operative time and complexity, the current study is the first to analyze changes in JPF as a means of differentiating tumor behavior, here ccRCC grade. One study has reported perinephric fat infiltration to be an independent prognostic factor for disease-free survival, particularly in pT3a RCC tumors [13]. Here, we use CTTA characterization of JPF surrounding ccRCC to assess intratumoral heterogeneity, a known feature of malignant tumor biology [3]. Heterogeneity on computed tomography (CT) can be quantified using texture analysis represented here by histogram analysis, GLCM, GLDM, and Fourier analysis which extracts information from CT images (unenhanced, contrast-enhanced and derived images such as CT perfusion) that may not be perceptible to the naked eye, and thus be missed during routine qualitative analysis. According to the AUC value of 0.75 with a 95% confidence interval (0.63–0.86), we see that measure of correlation coefficient on the sagittal plane in GLCM analysis had the best predictive value out of all other texture analysis tests in distinguishing between JPF surrounding low-grade versus high-grade ccRCC. If this finding is validated by further studies, radiomic analysis of JPF could potentially facilitate diagnosis, risk-assessment counseling and prognosis of ccRCC.

Limitations

Our single-center, retrospective study has limitations. First, the study was using data from a single type scanner from a single CT vendor, with the same imaging protocol. While, the similar experiment can be extended to other scanner and vendor types, caution is warranted, as variability in acquisition and processing techniques have been shown to affect radiomics performance [18]. Due to our stringent approach to acquire controlled data, our sample size (n = 83), while quite moderate, is comparable to similar exploratory studies [15]. In our study, we also had a lower number of high grade compared to low grade tumors. This reflects the distribution normally seen at our institute as well as in clinical practice elsewhere [16]. From a radiomics analysis standpoint, while we run the risk of overfitting, our model due to too many metrics [19], (n = 348) for our moderate sample size, the ratio of our feature space to sample size is also comparable to similar exploratory studies from other domains [15]. Some studies use feature selection techniques to reduce the number of metrics [20]; however, there is no consensus regarding the improvement of classification accuracy by performing feature selection. Improvements are mainly in terms of computation time. Additionally, this is an exploratory study. The focus is on the univariate descriptive analysis by showing the pattern of the association between radiomic metrics from different CECT phases and tumor grades. The data presented here need to be validated by a larger, prospective multi-center study.

There is no validated method to select the thickest or most optimal segment of JPF, so acquisition of 'best' segment was subjective. Also, currently, the segmentation step within our radiomic workflow is manual. We adopted the manual technique due to the lack of a reliable automated technique to perform the segmentation task consistently. While no subjective reader evaluation was performed, the same reader segmented all lesions. In an unrelated cohort of renal masses, we conducted an inter-rater agreement test for performing manual segmentation among 3 radiologists and reported an intra-class correlation coefficient of 0.97 $\pm$ 0.07, indicating good reliability and reproducibility of the segmentation results [Blinded]. For the purposes of this study, we did not analyze texture characteristics of the tumor itself, as this is a finding that has been previously evaluated by a number of researchers, including us [10, 14, 15]. The current study is a proof-of-concept, pilot study to evaluate whether there are radiomic differences in the JPF surrounding low- versus high-ccRCC could discriminate between the two categories of ccRCC. In our analysis, we demonstrate differences in JPF texture in a specific plane (e.g., coronal plane in the GLDM analysis or sagittal plane in the GLCM analysis) and not another. This was done to preserve the separability of texture metrics. The direction-invariant analysis performed as part of the 3D analysis averages these differences. While, it would have been interesting to explore correlations between radiomic metrics evaluated in our study and differences in histopathology, 82% of our retrospectively identified patient cohort had partial nephrectomy and pathologic evaluation of the perinephric fat was not feasible.

Through this pilot study, we aimed to differentiate high- and low-grade tumors even with a relatively small number of grade 4 tumors based on the analysis of the JPF surrounding them. To this end, we did not control for the type 1 error rate. Subsequently, we did not conduct multivariate analysis nor correct for multiple comparisons since our analysis was designed to be descriptive. Multivariate analysis with variable selection to control for multiple comparisons can be implemented by sophisticated statistical methods such as Least Absolute Shrinkage and Selection Operator (LASSO). However, this would be better suited for studies with larger sample sizes. For such multivariate analyses, we should have large enough sample

size to split data into training and testing data, then evaluate the performance by the independent testing dataset. Conducting naïve multivariate analysis or multiple comparison correction will not reach the same scientific quality as the LASSO model with independent testing data. In conclusion, our preliminary finding showed that some radiomic metrics can differentiate high- and low-grade tumors even with small number of grade 4 tumors based the textural analysis of the JPF surrounding them. This finding encourages the effort for pursuing future studies with a larger sample size.

Conclusion

Texture analysis methods such as Fourier analysis, GLDM, and Histogram analysis show statistically significant different metrics to delineate radiomics characteristics of JPF surrounding low-grade (1–2) versus high-grade (3–4) ccRCC are. Results of 1st order statistical tests show increased textural heterogeneity in JPF surrounding higher grade 3–4 ccRCC, as indicated by increased kurtosis and positive skewness in Histogram analysis, and increased complexity index in Fourier analysis. 2nd order statistical test GLDM showed increased textural heterogeneity in the JPF surrounding higher grade 3–4 ccRCC, as indicated by decreased MCC in GLDM analysis. To this end, establishment of reliable (robust, reproducible and repeatable) radiomic metrics which can be used in multi-center studies will further validate our results using a larger patient cohort may support the concept of using CTTA metrics of the JPF as an aid to grade ccRCC.

Acknowledgements The authors acknowledge FUJIFILM Medical Systems USA, Inc. for the use of their Synapse® 3D software for completing this work.

Author contributions TG is the first author and drafted the manuscript. She manually segmented the JPF in Synapse 3D. BV performed data processing and reviewed manuscript. DH aided in CT analysis. SC performed the statistical analysis. MA performed pathological correlation. MA provided urological clinical significance. VD supervised the study, as well as reviewed and edited manuscript. All authors read and approved the final manuscript.

Funding The project did not receive any funding.

Compliance with ethical standards

Conflict of interest Dr. Vinay Duddalwar serves as a consultant to Intuitive Surgical and as an advisor to DeepTek. Dr. Monish Aron serves as a consultant to Intuitive Surgical. The other authors have no conflict of interest with respect to the work presented in this manuscript.

Research involving human participants and/or animals All procedures performed in studies involving human participants were in accordance with the ethical standards of the institutional and/or national research committee and with the 1964 Helsinki declaration and its later amendments or comparable ethical standards. For this type of study, formal consent is not required.

Informed consent Informed consent was obtained from all individual participants included in the study.

References

1. Siegel R, DeSantis C, Virgo K, Stein K, Mariotto A, Smith T, et al. Cancer treatment and survivorship statistics, 2012. CA Cancer J Clin. 2012;62(4):220–41.
2. Xing T, He H. Epigenomics of clear cell renal cell carcinoma: mechanisms and potential use in molecular pathology. Chin J Cancer Res. 2016;28(1):80–91.
3. Burrell RA, McGranahan N, Bartek J, Swanton C. The causes and consequences of genetic heterogeneity in cancer evolution. Nature. 2013;501(7467):338–45.
4. Shuch B, Amin A, Armstrong AJ, Eble JN, Ficarra V, Lopez-Beltran A, et al. Understanding pathologic variants of renal cell carcinoma: distilling therapeutic opportunities from biologic complexity. Eur Urol. 2015;67(1):85–97.
5. Casbas-Hernandez P, Sun X, Roman-Perez E, D'Arcy M, Sandhu R, Hishida A, et al. Tumor intrinsic subtype is reflected in cancer-adjacent tissue. Cancer Epidemiol Biomarkers Prev. 2015;24(2):406–14.
6. Panis C, Victorino VJ, Herrera AC, Cecchini AL, Simao AN, Tomita LY, et al. Can Breast Tumors Affect the Oxidative Status of the Surrounding Environment? A Comparative Analysis among Cancerous Breast, Mammary Adjacent Tissue, and Plasma. Oxid Med Cell Longev. 2015;2015:6429812.
7. Macleod LC, Hsi RS, Gore JL, Wright JL, Harper JD. Perinephric fat thickness is an independent predictor of operative complexity during robot-assisted partial nephrectomy. J Endourol. 2014;28(5):587–91.
8. Anderson KM, Lindler TU, Lamberton GR, Baron PW, Ojogho OK, Baldwin DD. Laparoscopic donor nephrectomy: effect of perirenal fat upon donor operative time. J Endourol. 2008;22(10):2269–74.
9. Kocher NJ, Kunchala S, Reynolds C, Lehman E, Nie S, Raman JD. Adherent perinephric fat at minimally invasive partial nephrectomy is associated with adverse peri-operative outcomes and malignant renal histology. BJU Int. 2016;117(4):636–41.
10. Varghese BA HD, Cen SY, Desai BB, Yap, FY, Gill I, Desai M, et al. . Fast fourier transform based analysis of renal masses on contrast-enhanced computed tomography images for grading of tumor. International Society for Optics and Photonics2017. p. 101600J-J-8.
11. Yu H, Scalera J, Khalid M, Touret AS, Bloch N, Li B, et al. Texture analysis as a radiomic marker for differentiating renal tumors. Abdom Radiol (NY). 2017.
12. Just N. Improving tumour heterogeneity MRI assessment with histograms. Br J Cancer. 2014;111(12):2205–13.
13. Yoo C, Song C, Hong JH, Kim CS, Ahn H. Prognostic significance of perinephric fat infiltration and tumor size in renal cell carcinoma. J Urol. 2008;180(2):486–91; discussion 91.
14. Skogen K, Ganeshan B, Good C, Critchley G, Miles K. Measurements of heterogeneity in gliomas on computed tomography relationship to tumour grade. J Neurooncol. 2013;111(2):213–9.

15. Yang L, Dong D, Fang M, Zhu Y, Zang Y, Liu Z, et al. Can CT-based radiomics signature predict KRAS/NRAS/BRAF mutations in colorectal cancer? Eur Radiol. 2018;28(5):2058–67.
16. Chen C, Kang Q, Xu B, Guo H, Wei Q, Wang T, et al. Differentiation of low- and high-grade clear cell renal cell carcinoma: Tumor size versus CT perfusion parameters. Clin Imaging. 2017;46:14–9.
17. Qian BZ, Pollard JW. Macrophage diversity enhances tumor progression and metastasis. Cell. 2010;141(1):39–51.
18. Mackin D, Fave X, Zhang L, Fried D, Yang J, Taylor B, et al. Measuring Computed Tomography Scanner Variability of Radiomics Features. Invest Radiol. 2015;50(11):757–65.
19. Duda RO, Hart PE, Stork DG. Pattern Classification (2nd Edition): Wiley-Interscience; 2000.
20. Haury AC, Gestraud P, Vert JP. The influence of feature selection methods on accuracy, stability and interpretability of molecular signatures. PLoS One. 2011;6(12):e28210.